

SCHOOL OF MATERIALS AND MINERAL RESOURCES ENGINEERING  
UNIVERSITI SAINS MALAYSIA

SUPERIOR HARDNESS OF ZIRCONIA TOUGHENED ALUMINA CERAMICS  
THROUGH CO-ADDITION OF MAGNESIUM OXIDE AND LANTHANUM  
OXIDE

By

KONG CHEE XIAN

Supervisor : Professor Dr. Hj. Zainal Arifin Ahmad

Co-supervisor : Dr. Nik Akmar Rejab

Dissertation submitted in partial fulfillment  
of the requirements for the degree of Bachelor of Engineering with Honours  
(Materials Engineering)  
Universiti Sains Malaysia

JUNE 2018

## DECLARATION

I hereby declare that I have conducted, completed for the research work and written the dissertation entitled Superior Hardness of Zirconia Toughened Alumina Ceramics through Co-addition of Magnesium oxide and Lanthanum oxide. I also declare that it has not been previously submitted for the award of any degree or diploma or other similar title of this for any other examining body or university.

Name of Student: Kong Chee Xian

Signature:

Date:

Witnessed by

Supervisor: Professor Dr. Hj. Zainal Arifin Ahmad

Signature:

Date:

## **ACKNOWLEDGEMENTS**

First of all, I would like to express my gratitude towards School of Materials and Mineral Resources Engineering for providing me with the necessary equipment's and resources required to complete my project. Special thanks go to Dean of School of Materials and Mineral Resources Engineering, Professor Dr. Zuhailawati Hussain for giving me an opportunity to complete my degree.

Next, I would like to take this opportunity to thank my supervisor, Professor Dr. Hj. Zainal Arifin Ahmad for the suggestion, advice and guidance throughout the implementation of my final year research project.

In addition, I also would like to express my gratefulness to Dr. Nik Akmar Rejab who acted as my co-supervisor that has given me plenty of guidance, advice and explanation in my entire project.

For the technical perspective, I would like to thank to Mr. Abdul Rashid Selamat, Mr. Shahid Abdul Jalal, Mr. Sharul Ami Zainal Abidin and Mr. Mohd. Farid Abdul Rahim whom are technicians from School of Materials and Mineral Resources Engineering.

Last but not least, I would like to thank my parents Mr. Kong Wai Mun and Mdm. Lee Yoke Ken for their boundless support to me.

## TABLE OF CONTENTS

<b>Contents</b>	<b>Page</b>
CHAPTER 1 INTRODUCTION	
1.1 Introduction	1
1.2 Problem Statement	3
1.3 Research Objectives	4
1.4 Project Approaches	4
CHAPTER 2 LITERATURE REVIEW	
2.1 Introduction	5
2.2 Research Background	6
2.3 Research Gap	8
2.4 Zirconia Toughened Alumina (ZTA)	11
2.5 Toughening Mechanism in ZTA System	13
2.6 Limitation of ZTA	14
2.7 Magnesium Oxide (MgO)	15
2.8 Lanthanum Oxide ( $\text{La}_2\text{O}_3$ )	17
2.9 Fabrication of ZTA	19
2.10 Sintering	20
2.11 Uniaxial Pressing Method	22
2.12 Characterization	23
2.12.1 X-ray Diffraction (XRD)	23
2.12.2 Microstructure Observations	25
2.12.3 Fracture Toughness Evaluation with Large Cracks	29

2.12.4 Fracture Toughness Evaluation with Small Cracks	30
2.12.5 Relationship between Vickers Hardness and Fracture Toughness	30
CHAPTER 3 MATERIALS AND METHIDODOLOGY	
3.1 Introduction	35
3.2 Experimental Design	35
3.2.1 Experimental Description	36
3.3 Experimental Procedure	38
3.3.1 Weighing	38
3.3.2 Mixing	38
3.3.3 Drying	39
3.3.4 Pressing	39
3.3.5 Sintering	39
3.4 Characterization	40
3.4.1 Microstructure Observation	40
3.4.2 Bulk Density and Porosity Measurement	41
3.4.3 Vickers Hardness and Indentation Fracture Resistance	42
3.4.4 XRD Analysis	43
3.5.5 Optimization of La <sub>2</sub> O <sub>3</sub> wt.% Addition on ZTA/MgO Ceramics	43
CHAPTER 4 RESULTS AND DISCUSSION	
4.1 Introduction	44
4.2 The Effect of Addition of La <sub>2</sub> O <sub>3</sub> on Properties and Microstructure of ZTA/MgO	44
4.2.1 Macro Observation	44

4.2.2 X-ray Diffraction Analysis	44
4.2.3 Microstructure Observations	48
4.2.3.1 Microstructure Analysis on ZTA/MgO/ La <sub>2</sub> O <sub>3</sub>	49
4.3 The Effect of Addition of La <sub>2</sub> O <sub>3</sub> on the Mechanical Properties of ZTA/MgO	52
4.4.1 Bulk Density and Porosity Measurement	52
4.3.2 Vickers Hardness and Indentation Fracture Resistance Analysis	55
4.4 Optimization of the weight fraction addition of La <sub>2</sub> O <sub>3</sub> in ZTA/MgO ceramics	59
4.4.1 Bulk Density and Porosity Measurement	59
4.4.2 Vickers Hardness and Indentation Fracture Resistance Analysis	60
4.4.3 XRD Analysis on the Optimization Samples	62
4.4.4 Microstructural Analysis on the Optimization Samples	66
CHAPTER 5 CONCLUSION AND RECOMMENDATION	
5.1 Conclusion	69
5.2 Suggestion for Future Research	70
References	71

## LIST OF FIGURES

Figure 2.1	Variety of tools materials in high speed machining (Liu & Ai, 2005)	6
Figure 2.2	Micrographs for (a) monolithic Al <sub>2</sub> O <sub>3</sub> and (b) 80 wt.% Al <sub>2</sub> O <sub>3</sub> /20 wt.% YSZ (Azhar <i>et al.</i> , 2010).	12
Figure 2.3	EDX analysis of the ZTA/CeO <sub>2</sub> /MgO ceramic added with 3 wt.% CaCO <sub>3</sub> , (a) Al <sub>2</sub> O <sub>3</sub> , (b) hibonite, and (c) YSZ (Rejab <i>et al.</i> , 2016).	12
Figure 2.4	Transformation toughening mechanism of zirconia (Edward & Russell, 2005).	13
Figure 2.5	Vickers hardness of ZTA ceramics insets as a function of MgO wt.% (Azhar <i>et al.</i> , 2010).	15
Figure 2.6	Fracture toughness of the ZTA cutting inserts as a function of MgO wt.% (Azhar <i>et al.</i> , 2010).	16
Figure 2.7	SEM images of (a) ZTA ceramics with 12.5 wt.% LaAl <sub>11</sub> O <sub>18</sub> , (b) ZTA ceramics with 37.5 wt.% LaAl <sub>11</sub> O <sub>18</sub> (Naga <i>et al.</i> , 2016).	17
Figure 2.8	Effect of LaAl <sub>11</sub> O <sub>18</sub> content on (a) Bending strength (b) Vickers Hardness and (c) Fracture toughness of ZTA composite (Naga <i>et al.</i> , 2016).	18
Figure 2.9	For powder compact, microstructural changes during sintering. (a) Powder particles after pressing, (b) Particle coalescence and pore formation as sintering begins and (c) As sintering proceeds, the pores change size and shape (De Jonghe & Rahaman, 2003).	21
Figure 2.10	Figure 2.10: Schematic representation of the sintered mechanism for a system of two particles (De Jonghe & Rahaman, 2003)	22
Figure 2.11	Schematic diagram of the uniaxial pressing method (Riedel & Chen, 2012)	23

Figure 2.12	XRD pattern of the $\text{Al}_2\text{O}_3/\text{LaAl}_{11}\text{O}_{18}/\text{ZrO}_2$ ceramics with different content of $\text{LaAl}_{11}\text{O}_{18}$ : ( $L_0$ ) 0 wt.% of $\text{LaAl}_{11}\text{O}_{18}$ , ( $L_1$ ) 12.5 wt.% of $\text{LaAl}_{11}\text{O}_{18}$ , ( $L_2$ ) 25 wt.% of $\text{LaAl}_{11}\text{O}_{18}$ , ( $L_3$ ) 37.5 wt.% of $\text{LaAl}_{11}\text{O}_{18}$ and ( $L_4$ ) 50 wt.% of $\text{LaAl}_{11}\text{O}_{18}$ (Naga <i>et al.</i> , 2016)	24
Figure 2.13	Result of XRD analysis on ZTA/MgO sintered body with different MgO wt.% (Azhar <i>et al.</i> , 2010)	25
Figure 2.14	Microstructure of: (a) $\text{Al}_2\text{O}_3$ ceramics with 30 mass% of stabilized $\text{ZrO}_2$ , and (b) standard $\text{Al}_2\text{O}_3$ ceramics SN80 (Smuk <i>et al.</i> 2003).	26
Figure 2.15	SEM micrographs of the studied composites microstructure: (a) elongated alumina particles of ZTA ceramics with 37.5 wt.% of $\text{LaAl}_{11}\text{O}_{18}$ , (b) t- and m- $\text{ZrO}_2$ particles of ZTA ceramics with 37.5 wt.% of $\text{LaAl}_{11}\text{O}_{18}$ , (c) $\text{LaAl}_{11}\text{O}_{18}$ grains with rippled surface and (d) the transformation of rippled grains into rod like particles (Naga <i>et al.</i> , 2016).	27
Figure 2.16	SEM micrographs of cutting insert surface (a) 0 wt.% MgO, (b) 0.3 wt.% MgO, (c) 0.5 wt.% MgO, (d) 0.7 wt.% MgO, (e) 0.9 wt.% MgO and (f) 1.0 wt.% MgO (Azhar <i>et al.</i> , 2010)	28
Figure 2.17	Geometry of Vickers hardness test (El-Sherbiny <i>et al.</i> , 2012).	31
Figure 2.18	Configurations of the Palmqvist cracks for the Vickers hardness indentation (Smuk <i>et al.</i> , 2003).	31
Figure 3.1	Flowchart to study the effect of $\text{La}_2\text{O}_3$ additives on the ZTA/MgO ceramic	37
Figure 3.2	Heating profile for sintering	39
Figure 3.3	Heating profile used for thermal etching	41
Figure 4.1	Overall XRD diffractograms of ZTA/MgO ceramic composites with different $\text{La}_2\text{O}_3$ wt.%.	45
Figure 4.2	SEM micrographs ZTA/MgO with different weight fraction of $\text{La}_2\text{O}_3$ wt.%: a) 0 wt.%, b) 0.1 wt.%, c) 0.3 wt.%, d) 0.5 wt.%, e) 0.7 wt.%, f) 1.0 wt.%, g) 3.0 wt.%, h) 5.0 wt.%, i) 7.0 wt.% and j) 10 wt.%	49



Figure 4.3	Results of bulk density and percentage of porosity for ZTA/MgO as a function of La <sub>2</sub> O <sub>3</sub> ceramic	53
Figure 4.4	Results of Vickers hardness and indentation fracture resistance for ZTA/MgO as a function of La <sub>2</sub> O <sub>3</sub> wt.%.	55
Figure 4.5	Results of bulk density and percentage of porosity for optimization of ZTA/MgO as a function of La <sub>2</sub> O <sub>3</sub> wt.%	59
Figure 4.6	Results of Vickers hardness and indentation fracture resistance for optimization of ZTA/ MgO as a function of La <sub>2</sub> O <sub>3</sub> wt.%.	60
Figure 4.7	Overall XRD diffractograms of ZTA/MgO ceramic composites with different La <sub>2</sub> O <sub>3</sub> wt.% for optimization	63
Figure 4.8	SEM micrograph of ZTA/MgO with different weight fraction of La <sub>2</sub> O <sub>3</sub> for optimization: a) 0.75 wt.%, b) 0.80 wt.%, c) 0.85 wt.%, d) 0.90 wt.% and e) 0.95 wt.%.	67
Figure 4.9	Crack path in the ZTA/MgO with 0.85 wt.% La <sub>2</sub> O <sub>3</sub> induced by Vickers indentation.	68

## LIST OF TABLES

Table 2.1	Previous researches to improve the mechanical properties of ZTA system.	9
Table 2.2	Mechanical characteristic of Al <sub>2</sub> O <sub>3</sub> /YSZ sintered composites (Cesari <i>et al.</i> , 2006)	33
Table 3.1	Weight for raw materials used in mixing	38
Table 4.1	Quantitative results of ZTA/MgO ceramic composites with different La <sub>2</sub> O <sub>3</sub> wt.%.	46
Table 4.2	Result of bulk density and percentage of porosity for ZTA/MgO as a function of La <sub>2</sub> O <sub>3</sub> ceramic	53
Table 4.3	Average results of Vickers hardness and indentation fracture resistance for ZTA/MgO as a function of La <sub>2</sub> O <sub>3</sub> wt.%.	56
Table 4.4	Results of bulk density and percentage of porosity for optimization of ZTA/MgO as a function of La <sub>2</sub> O <sub>3</sub> wt.%	60
Table 4.5	Results of Vickers hardness and indentation fracture resistance for optimization of ZTA/MgO as a function of La <sub>2</sub> O <sub>3</sub> wt.%.	60
Table 4.6	Quantitative results of ZTA/MgO as a function of La <sub>2</sub> O <sub>3</sub> wt.% for optimization.	62

## LIST OF SYMBOLS

$a$	Half of the indentation diagonal length
$E$	Modulus Young
$HV$	Vickers hardness
$K_{IC}$	Fracture toughness
$K_{IFR}$	Indentation fracture resistance
$l$	Length of the radiant crack
$D_i$	Initial length of sample
$D_f$	Final length of sample
(t)	Tetragonal phase
(m)	Monoclinic phase
$\rho_b$	Bulk density

## LIST OF ABBREVIATIONS

CIP	Cold isostatic pressing
EDX	Energy dispersive X-ray spectroscopy
FESEM	Field emission scanning electron microscope
HIP	Hot isostatic pressing
ICDD	International centre for diffraction data
MWCNT	Multiwall carbon nanotubes
SEM	Scanning electron microscope
wt. %	Weight percentage
XRD	X-ray diffraction
YSZ	Yttria stabilized zirconia
ZTA	Zirconia toughened alumina

# KEKERASAAN UNGGUL SERAMIK ZTA MELALUI PENAMBAHAN OKSIDA MAGNESIUM dan OKSIDA LANTANUM

## ABSTRAK

Penambahan MgO dalam seramik alumina diperkuat zirconia (ZTA) menunjukkan dampak positif dari segi kekerasan Vickers sebanyak 1710 HV tetapi ia mempunyai nilai rintangan patah lekukan ( $K_{\text{IFR}}$ ) hanya sebanyak  $3.38 \text{ MPa}\cdot\sqrt{\text{m}}$ . Puncanya adalah pembentukan fasa  $\text{MgAl}_2\text{O}_4$  yang mempunyai intrinsik  $K_{\text{IFR}}$  yang rendah dalam sistem ZTA/MgO. Mata permotong seramik yang berprestasi tinggi sepatutnya mempunyai kekerasan and  $K_{\text{IFR}}$  yang tinggi. Oleh sebab itu, penambahan  $\text{La}_2\text{O}_3$  dalam ZTA dianggap sebagai satu pendekatan untuk meningkatkan  $K_{\text{IFR}}$  bagi seramik berdasarkan alumina. Bahan mula disediakan dengan penambahan  $\text{La}_2\text{O}_3$  dari 0.1% berat hingga 10.0% berat ke dalam ZTA/ 1.0% berat MgO seramik. Campuran dimampatkan dengan pemampat hidraulik dalam acuan silinder untuk menghasilkan bar segi empat. Bar kemudian disinter pada suhu  $1600 \text{ }^\circ\text{C}$  dengan tempoh rendaman selama 4 jam. Setelah mikrostruktur seramik dan pembentukan fasa diperhatikan, ketumpatan pukal, peratus keliangan, kekerasan Vicker dan  $K_{\text{IFR}}$  diukur serta dikira. Dari keputusan kekerasan Vicker dan  $K_{\text{IFR}}$  diperolehi, proses penambahbaikan dijalankan dengan komposisi penambahan  $\text{La}_2\text{O}_3$  dari 0.7% berat hingga 1.0% berat untuk mendapatkan komposisi optimum bagi seramik ZTA/MgO/ $\text{La}_2\text{O}_3$ . Butir  $\text{Al}_2\text{O}_3$  yang lebih halus dapat dibentuk dengan penambahan  $\text{La}_2\text{O}_3$ . Antara muka yang kuat di antara butir  $\text{Al}_2\text{O}_3$  dan butir  $\text{LaAl}_{11}\text{O}_8$  terbentuk dan hasilnya seramik yang lebih padat dengan nilai kekerasan sebanyak 2028 HV. Selain itu, wujudnya butir  $\text{LaAl}_{11}\text{O}_8$  berbentuk batang dalam seramik ZTA/MgO meningkatkan  $K_{\text{IFR}}$  ke  $6.67 \text{ MPa}\cdot\sqrt{\text{m}}$ .

# SUPERIOR HARDNESS OF ZTA CERAMICS THROUGH CO-ADDITION OF MAGNESIUM OXIDE AND LANTHANUM OXIDE

## ABSTRACT

MgO addition into Zirconia toughened Alumina (ZTA) shown a positive impact on Vickers hardness (1710 HV) but only reduced the indentation fracture resistance ( $K_{IFR}$ ) (3.38 MPa. $\sqrt{m}$ ). The low  $K_{IFR}$  originated from the formation  $MgAl_2O_4$  phase in the ZTA /MgO system decreased the  $K_{IFR}$  of the ceramics due to the low intrinsic indentation fracture resistance of  $MgAl_2O_4$ . To develop a high performance cutting insert, the ceramics must acquire both high hardness and  $K_{IFR}$  value. Hence, addition of  $La_2O_3$  in ZTA seem to be an approach as  $La_2O_3$  are capable of improving the  $K_{IFR}$  of alumina-based ceramics. The mixtures were prepared with addition of  $La_2O_3$  (0.1 wt.% to 10.0 wt.%) to ZTA/1.0 wt.% MgO. The mixtures were pressed to a rectangular bar at 1600 °C for 4 hours to observe its effect on microstructure, phases formation, density, porosity and finally measurement of hardness and  $K_{IFR}$ . From the hardness and  $K_{IFR}$  result obtained, optimization was carried out to tune with the addition of  $La_2O_3$  content (0.7 wt.% - 1.0 wt.%) for better  $K_{IFR}$  with slight reduction of the hardness value. The addition of  $La_2O_3$  shown a significant effect on the formation of finer  $Al_2O_3$  grains, creating strong interface between the  $Al_2O_3$  grains and  $LaAl_{11}O_8$  grains result in denser ZTA/MgO ceramics of hardness of 2028 HV. Also, the presence of rod like  $LaAl_{11}O_8$  grains in the ZTA/MgO ceramics improved the  $K_{IFR}$  up to 6.67 MPa. $\sqrt{m}$ .

# CHAPTER 1

## INTRODUCTION

### 1.1 Introduction

Machining is a one of the major process in manufacturing routes. The performance of machining process can be determined in terms of tools life, depth of cutting, cutting speed as well as surface finishing during operation. The breakthrough of this area is that the increase of the application advanced ceramic materials in the machining operation. Despite of all those advanced ceramic, alumina ceramic has always been the favorite one due to the superior properties like high strength, high hardness, high corrosion and heat resistance as well as good thermal stability (Yao *et al.*, 2010). Thus, they also used in hash and abrasive wear environment like ball mills, grinders mixer and coal chutes.

Despite of all those excellent properties, the Achilles' heel of alumina based cutting tools is poor fracture toughness. This makes them susceptible to failure during machining operation such as chipping (Azhar *et al.*, 2009). Therefore, additives such as yttria stabilized zirconia (YSZ), ceria (CeO<sub>2</sub>), silver and titanium carbide were used to improve the fracture toughness of alumina based ceramics (Azhar *et al.*, 2012). By doing so, it not only can increase the performance of the cutting tools but also their lifespans.

Previous study from Azhar *et al.* (2010) shown that the fracture toughness and wear resistance of ceramic cutting inserts with Al<sub>2</sub>O<sub>3</sub>/YSZ system improved significantly. In this study, 20 wt.% of YSZ addition produced the minimum wear area, while the fracture toughness values are increased up to 60 wt.% of YSZ addition. This is due to

the transformation strengthening process by tetragonal phase to monoclinic phase of YSZ in the alumina matrix.

Researches done by Azhar *et al.* (2010) and Mahmood *et al.* (2017) shown the presence of MgO in the alumina matrix will affect the mechanical properties of ZTA. Addition of 0.7 wt.% of MgO in ZTA system produced minimum wear area of 0.019 mm<sup>2</sup> with Vickers hardness of 1712 HV. The incorporation of MgO into ZTA increased the hardness by reducing Al<sub>2</sub>O<sub>3</sub> grain size (Azhar *et al.*, 2010). Also, addition of 1 wt.% MgO in the ZTA system produced ceramic with fracture toughness of 6.29 MPa.√m providing that the fracture toughness of pure ZTA is 4.00 MPa.√m (Mahmood *et al.*, 2017).

Lanthanum aluminate (LaAl<sub>11</sub>O<sub>18</sub>) has an anisotropic growth habit and is suitable for toughening reinforcement. By adding the rod like particles into ZrO<sub>2</sub> transformation toughened ceramics, impressive results have been reported by Guo *et al.* (2002). The mechanical properties of ZTA ceramics were improved by the LaAl<sub>11</sub>O<sub>18</sub> with strength over 500 MPa and fracture toughness of 7 MPa.√m. However, the properties of ceramics decrease with the increase of aluminate content. This is because of the hardness and Young's modulus of aluminates are much lower than corundum, (Guo *et al.*, 2002).

Fracture toughness is criteria that prevent the cutting tools from premature failure. Cutting tools with low fracture toughness always fail early during the machining operation.



## 1.2 Problem Statement

ZTA not only finds application in heat engines, rocket nozzles and cutting tools but also bushing and joint implants. This is because of its enhanced mechanical properties such as high strength, hardness and fracture toughness as well as high thermal stability and corrosion resistance (Subraya *et al.*, 2008).

Despite with the reinforcement of YSZ, the fracture toughness of ZTA only improved to  $\sim 4.5 \text{ MPa}\cdot\sqrt{\text{m}}$  compared to monolithic  $\text{Al}_2\text{O}_3$ :  $3.9 \text{ MPa}\cdot\sqrt{\text{m}}$  (Casellas *et al.*, 2003). Previous researchers found that the metastable tetragonal phase of zirconia can be stabilized by incorporating with Yttrium(II) oxide ( $\text{Y}_2\text{O}_3$ ), Chromic oxide ( $\text{Cr}_2\text{O}_3$ ) or Cerium(III) oxide ( $\text{Ce}_2\text{O}_3$ ). The addition not only stabilized zirconia on  $\text{Al}_2\text{O}_3$  matrix but also promoting grain bridging and crack deflection (Elias *et al.*, 2004). Work done Azhar *et al.* (2010) shown that an addition of 0.7 wt.% of MgO in ZTA system produces ceramic with Vickers hardness of 1710 HV. However, this addition significantly reduced the fracture toughness of the ceramic due to the intrinsic nature of low fracture toughness of MgO. Also, Rejab *et al.* (2014) proved that the presence of  $\text{MgAl}_2\text{O}_4$  phase in the ZTA/ $\text{CeO}_2$  system with more than 5 wt.% addition decrease the fracture toughness of the ceramics because of low intrinsic indentation fracture resistance. Thus, other additives must be incorporated with the ZTA/MgO system and hence increase the hardness of the ceramic as well as reduce the drop of indentation fracture resistance.

Therefore,  $\text{La}_2\text{O}_3$  additives will be added into ZTA/MgO system to form ZTA/MgO/ $\text{La}_2\text{O}_3$  ceramics. This current study is to investigate the relationship of the amount of additives with the phases formed, microstructure and mechanical properties of ZTA ceramics system though uniaxial pressing.

### **1.3 Research Objectives**

- i. To investigate the effect of  $\text{La}_2\text{O}_3$  addition on the mechanical properties of ZTA/MgO ceramics.
- ii. To optimize the mechanical properties of  $\text{La}_2\text{O}_3$  addition into ZTA/MgO ceramics.

### **1.4 Project Approaches**

ZTA/MgO ceramic were fabricated with various  $\text{La}_2\text{O}_3$  wt.% addition and the changes were examined in terms of mechanical and microstructural properties. The ZTA consists of 80 wt.% of  $\text{Al}_2\text{O}_3$  and 20 wt.% of YSZ. 1 wt.% of MgO were added while the amount of  $\text{La}_2\text{O}_3$  were varied from 0 wt.% to 10.0 wt.%. Each batch of the mixture was mixed homogenously and dried for 24 hours. Drying process is carried out to remove the moisture content which will lead to formation of pores. The mixture is then uniaxially press into a rectangular shape bar with dimension of 12 mm x 54 mm x 5 mm (width x length x height) at 10 MPa with dwell time of 2 minutes. After that, the bars were sintered at 1600 °C. Properties such as density, percentage of porosity, microstructure observation, XRD analysis, Vickers hardness and fracture toughness were investigated. The purpose of microstructure observation is to investigate the relation between grain size and pores size of the sintered samples with their mechanical properties. Also, XRD analysis was carried out to identify the secondary phase present in the sintered samples. The second part of this experiment was to optimize the content of  $\text{La}_2\text{O}_3$  wt.% addition in ZTA/MgO ceramics.

## **CHAPTER 2**

### **LITERATURE REVIEW**

#### **2.1 Introduction**

This chapter covers research background as discussed in Section 2.2. Section 2.3 was about research gap and previous study done by the researches using different type of Zirconia Toughness Alumina (ZTA) system and fabrication route. Vickers hardness and indentation fracture resistance values were collected and tabulated for better comparison among each system. Also, the problem encountered for those researches were briefly discussed and the direction of this research was set. ZTA was compared with monolithic alumina in micrograph aspects as well as mechanical properties in Section 2.4. As for Section 2.5, toughening mechanism in ZTA system was briefly explained. The mechanism is induced due to the phase transformation of zirconia from tetragonal to monoclinic when the temperature changes. Limitation of ZTA was reveal in Section 2.6, and the approaches to improve the mechanical properties of ZTA was introduced. Magnesium oxide and lanthanum oxide which act as stabilizer was discussed in Sections 2.7 and 2.8 respectively. The fabrication and the sintering process of the samples are explained in Sections 2.9 and 2.10 for better understanding of the ceramics. In Section 2.11, the application of uniaxial pressing was explained and the characterization method which used to investigate the properties of the samples are also explained in Section 2.12 which include SEM, XRD, and Vickers hardness testing and fracture toughness analysis.

## 2.2 Research Background

The key link in cutting technology system is the edge tool. The tools are operated under high thermomechanical stresses such as dry cutting, high speed cutting and cutting of hard to cut materials. Generally, there is a basic dualism for all cutting tool materials. The harder and more wear resistant materials are usually less tough and unstable under alternating (Grigoriev *et al.*, 2012)

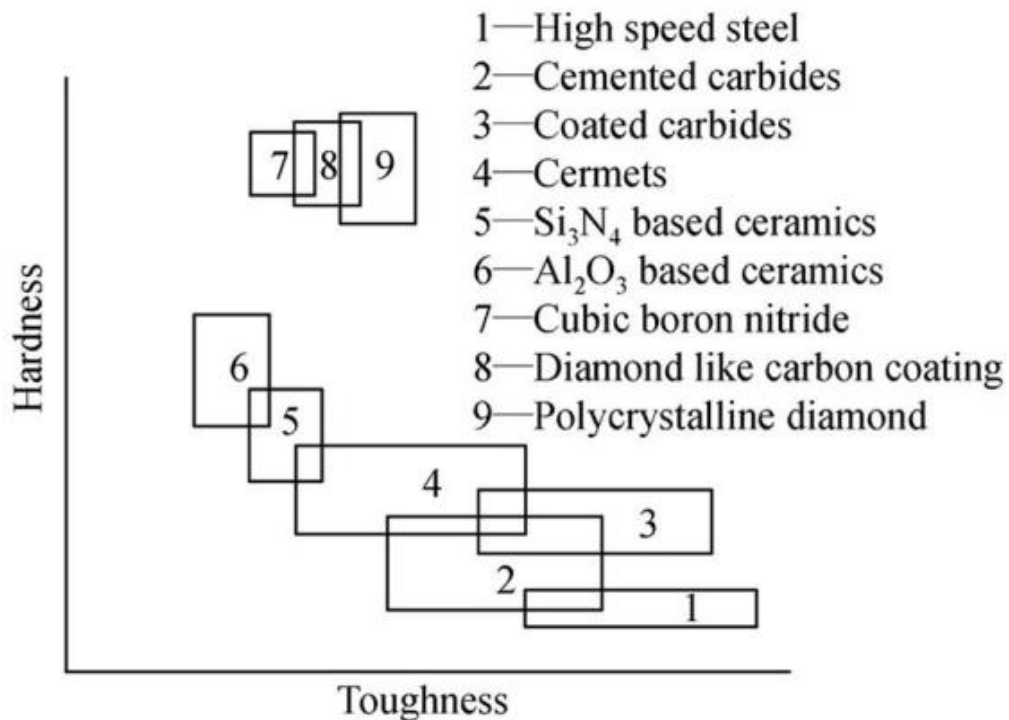


Figure 2.1: Variety of tools materials in high speed machining (Liu & Ai, 2005)

Due to high mechanical properties and low reactivity with steel at elevated temperature, ceramic became the favor of researches in the cutting inserts application. Low toughness and resistance to both mechanical and thermal shock limit their development in particular field. Fortunately, there has been significant improvement on the performance of ceramic cutting tools (Jack, 1986). Generally, there are two major

classes of ceramics cutting tools materials: alumina-based ceramics and silicon nitride-based ceramics.

Alumina-based ceramics has good chemical stability with ferrous metals and not susceptible to adhesion. As a comparison to tungsten carbide, the solubility of alumina in iron is only one fifth relatively. Thus, alumina-based ceramics acquired lower strength, fracture toughness, thermal conductivity, and thermal shock resistance (Liu & Ai, 2005). Therefore, the most suitable processing environment of alumina ceramic cutting tools is cutting hard and brittle metal materials with high speed, such as chilled cast iron or hardened steel, and copper alloy, graphite, engineering plastics and composite materials. The processing speed of the cast iron is as high as 900 m/min, and the cutting speed of the high temperature alloy is up to 120-240 m/min. Because the main ingredients of alumina ceramics are  $\text{Al}_2\text{O}_3$  and  $\text{Al}_2\text{O}_3$  has great affinity with aluminum, alumina ceramic cutting tool will severe wear when cutting aluminum and its alloy material. Therefore, alumina ceramic tools are not suitable for the processing of aluminum and aluminum alloy materials (Li & Li, 2017).

As for silicon nitride-based ceramics, they have high strength, fracture toughness, and thermal shock resistance. Also, they acquired a lower thermal expansion coefficient, Young's modulus, and chemical stability than alumina-based ceramics. However, they are not susceptible to adhesion with iron. Thus, silicon nitride-based ceramics are applied in the high-speed machining of cast iron most of the time (Liu & Ai, 2005).

In addition, Sialon ceramics ( $\text{Si}_3\text{N}_4\text{-Al}_2\text{O}_3$ ) have relatively high strength, fracture toughness, anti-oxidization, thermal conductivity, thermal shock resistance and creep

resistance at high temperature. Despite that, their low heat thermal resistance at high temperature makes them not suitable for steels machining. Thus, they are mainly used in the rough machining of cast iron and nickel-based alloy (Liu & Ai, 2005).

To improve the performance and wear resistance of ceramics tools to machine new work materials and composite. Researches shown their interest at ZTA ceramics and additives are applied to improve its fracture toughness.

### **2.3 Research Gap**

To improve the mechanical properties, additives were incorporated into the ZTA system to customize their microstructures.

Basically, hardness of most ZTA ceramics in those research was measured via Vickers hardness and fracture toughness were obtained via Niihara equation. An indentation load of 30 kgf was chosen, which was sufficient to produce a conveniently sized indentation for measurement through a built-in optical microscope, without occurrence of chipping. However, the method does not represent the actual fracture toughness. Thus, the fracture toughness is termed as indentation fracture resistance ( $K_{IFR}$ ). The  $K_{IFR}$  is applied as the measurement of the trend of the fracture toughness instead of the measuring actual values. Niihara equation measures the fracture toughness ( $K_{IC}$ ). And Miyazaki and Yoshizawa reported the  $K_{IFR}$  value for most ceramics is roughly proportional to the  $K_{IC}$ . This shown that the crack model is not overly incorrect. Table 2.1 shown researches' previous works for improving the mechanical properties of ZTA without diminishing properties of ZTA.

Table 2.1: Previous researches to improve the mechanical properties of ZTA system.

Reference	ZTA System	Fabrication Method	Vickers Hardness (HV)	Indentation Fracture Resistance (MPa. $\sqrt{m}$ )
Azhar <i>et al.</i> (2009)	ZTA	Uniaxial pressing	1630	4.07
Echeberria <i>et al.</i> (2010)	ZTA/0.0.1 MWCNT	Uniaxial pressing + HIP	1751	4.4
Azhar <i>et al.</i> (2010)	ZTA/0.7 MgO	Uniaxial pressing	1710	3.35
Azhar <i>et al.</i> (2012)	ZTA/0.6 Cr <sub>2</sub> O <sub>3</sub>	Uniaxial pressing	1683	4.73
Sktani <i>et al.</i> , (2014)	ZTA/0.5 CaCO <sub>3</sub>	Uniaxial pressing	1569	6.3
Rejab <i>et al.</i> (2013)	ZTA/5.0 CeO <sub>2</sub>	Uniaxial pressing	1688	8.38
Rejab <i>et al.</i> (2014)	ZTA/0.7 MgO/1.0 CeO <sub>2</sub>	Uniaxial pressing	1528	6.59
Hassan <i>et al.</i> (2015)	ZTA/0.6 Nb <sub>2</sub> O <sub>5</sub>	Sol-Gel	1792	6.19
Manshor <i>et al.</i> (2016)	ZTA/3.0 TiO <sub>2</sub> /0.6 Cr <sub>2</sub> O <sub>3</sub>	Uniaxial pressing	1681	7.15
Mahmood <i>et al.</i> (2017)	ZTA/0.5 TiO <sub>2</sub> /1.0 MgO	Uniaxial pressing	1637	9.86
Manshor <i>et al.</i> (2017)	ZTA/3.0 TiO <sub>2</sub> /0.6 Cr <sub>2</sub> O <sub>3</sub>	Uniaxial pressing + Microwave sintering	1803.4	9.61
Rejab <i>et al.</i> (2017)	ZTA/5.0 CeO <sub>2</sub>	Uniaxial pressing + HIP	1838.3	8.92

From those work done by the researches, it shown that they can either improve the hardness at the expense of reduction of indentation fracture resistance or vice versa. Hence, it is crucial to design a good ZTA system with both high value of hardness and indentation fracture resistance. It will be economical if the processing route is via conventional powder fabrication with uniaxial pressing.

Thus, ZTA/MgO system is taken in account in this particular research as it acquires relatively high hardness but low indentation fracture resistance value.  $\text{La}_2\text{O}_3$  was added as additive to improve the indentation fracture resistance of ZTA/MgO system. This is because  $\text{ZrO}_2$  is compatible with  $\text{Al}_2\text{O}_3$  and  $\text{LaAl}_{11}\text{O}_{18}$  and it can be used as a second reinforcing phase for  $\text{LaAl}_{11}\text{O}_{18}/\text{Al}_2\text{O}_3$  composites. The incorporation rod like  $\text{LaAl}_{11}\text{O}_{18}$  phase into ZTA ceramics decreases the sintering temperature and increases their indentation fracture resistance. The main toughening mechanisms are crack bridging and crack deflection together with residual thermal stresses (Naga *et al.*, 2016). Also, Guo *et al.* (2001) shown rod like grains enhances the sintering process at low sintering temperature. The produced composites showed high fracture and bending strength together with a high resistance to subcritical crack growth.

The combined effect of MgO and  $\text{La}_2\text{O}_3$  on the properties of ZTA is not well studied in previous researches. Thus, this work highlighted powder compaction for ZTA with MgO and  $\text{La}_2\text{O}_3$  addition simultaneously to achieve better mechanical properties. Separately addition of MgO and  $\text{La}_2\text{O}_3$  can improve the properties of  $\text{Al}_2\text{O}_3$  based composite materials. The effect of incorporating both MgO and  $\text{La}_2\text{O}_3$  to ZTA on the physical, mechanical and microstructural properties were investigated in this research.



## 2.4 Zirconia Toughened Alumina (ZTA)

Zirconia toughened alumina (ZTA) is an alumina matrix composite ceramic where alumina is the primary phase (70 - 95%) and zirconia is the secondary phase (30% - 5%). This ceramic combines the advantageous properties of monolithic alumina and zirconia. In this case, most zirconia is retained in the tetragonal phase, the addition results in higher strength and indentation fracture resistance with slight reduction in hardness and elastic modulus than the monolithic alumina ceramics. In addition, zirconia toughened alumina ceramics retained the excellent wear resistance and low susceptibility to stress assisted degradation of high performance alumina ceramics (Kurtz *et al.*, 2014). According to Maiti and Sil (2011), ZTA has been one of the most successful commercial ceramic based cutting inserts which fully utilize the outstanding properties of zirconia.

As for the mechanical properties aspect, ZTA is highly dependent on their microstructures. This means it can be designed in terms of specific applications by controlling the powder preparation and densification processes. From Figure 2.2, it is significant that ZTA has a denser microstructure compared to that of monolithic alumina. Since ZTA has less porosity in the microstructure, it has higher strength than alumina. This is because the pores will act as the point of crack initiation. Furthermore, the amount of YSZ in ZTA will influence its properties. Research done by Azhar *et al.* (2009) stated that the fracture toughness of ZTA increases with the increase of addition for YSZ till 60 wt.%. Once the amount additives exceed 60%, there will be cracks and large grains in the microstructure, inhibiting the transformation toughening mechanism from taking place.

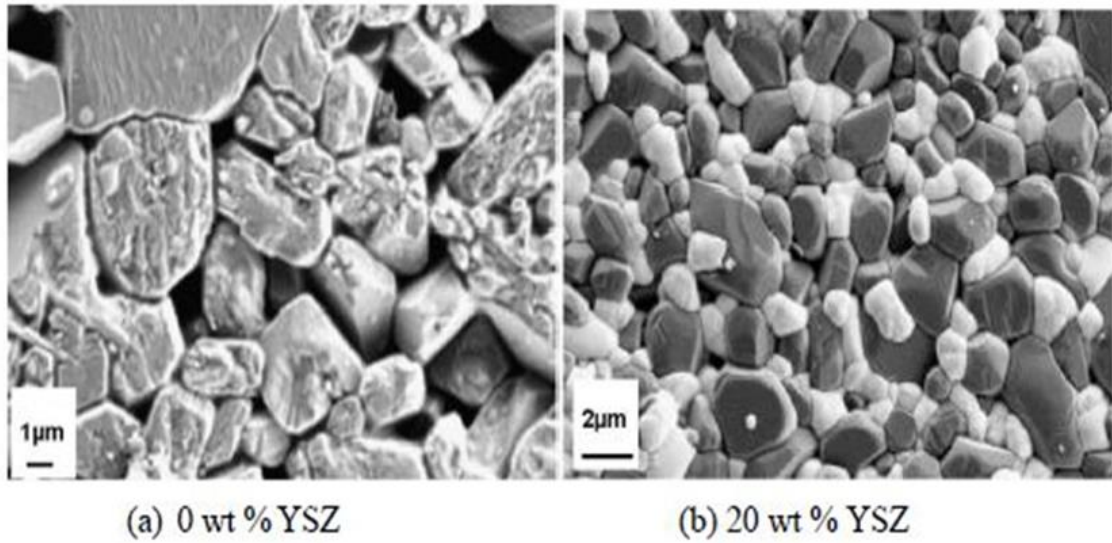


Figure 2.2: Micrographs for (a) monolithic  $\text{Al}_2\text{O}_3$  and (b) 80 wt.%  $\text{Al}_2\text{O}_3$ /20 wt.% YSZ (Azhar *et al.*, 2010).

Figure 2.3 shown a nice distribution of distribution of  $\text{ZrO}_2$  grains embedded within  $\text{Al}_2\text{O}_3$  and  $\text{CaAl}_{12}\text{O}_{19}$  grains or at grain boundaries. The dark grey platelet indicated  $\text{Al}_2\text{O}_3$  while the white equiaxial grains represent YSZ.

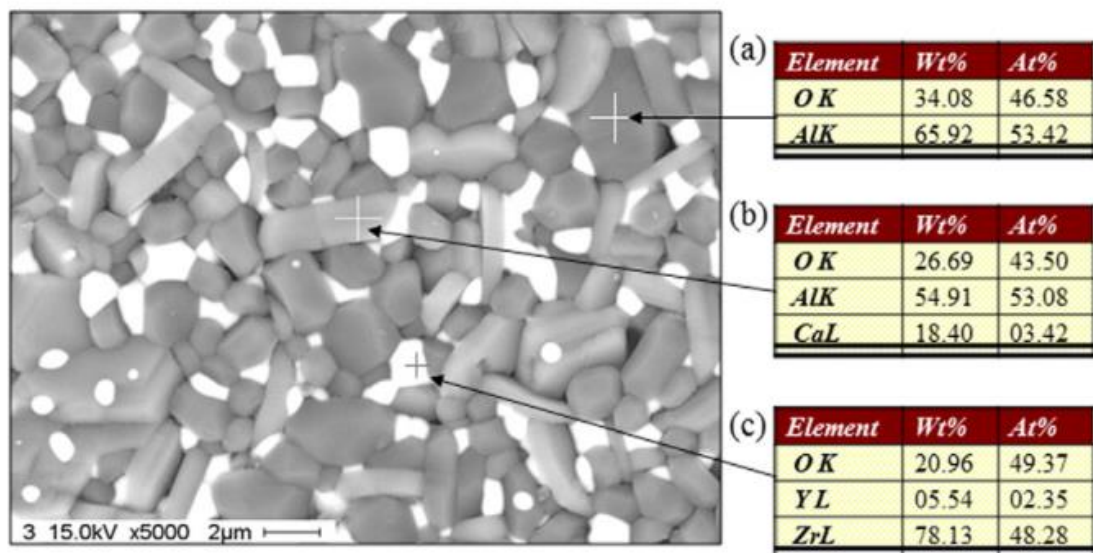


Figure 2.3: EDX analysis of the ZTA ceramic added with 3 wt.%  $\text{CaCO}_3$ , (a)  $\text{Al}_2\text{O}_3$ , (b) hibonite, and (c) YSZ (Rejab *et al.*, 2016).

## 2.5 Toughening Mechanism in ZTA System

According to Basu (2005), transformation toughening takes place when metastable  $t\text{-ZrO}_2$  transform to stable  $m\text{-ZrO}_2$  under tensile stress condition at propagating crack. Under isothermal conditions, the martensitic tetragonal to monoclinic transformation can be induced by cooling or external loading. Thermally induced transformation control the amount of tetragonal phase that can be retained after thermal cycling, the stress induced martensitic transformation enhances the toughness of zirconia ceramics (Basu, 2005)

To retain the tetragonal phase, dopants such as calcia (CaO), magnesia (MgO), yttria ( $\text{Y}_2\text{O}_3$ ), or ceria ( $\text{CeO}_2$ ) are added in specific proportions. Once the right amount of component is added, a fully stabilized cubic phase can be produced. If 3 wt.% to 5 wt.% were added, a partially stabilized zirconia is produced. The tetragonal zirconia phase is stabilized, but under stress, the phase may change to monoclinic, resulting in 3% of volumetric expansion. This dimensional change keeps energy away from the crack and prevent crack propagation. This is called transformation toughening as shown in Figure 2.4. Also, a compressive stress is created around the particle inhibiting the crack growth (Edward & Russell, 2005).

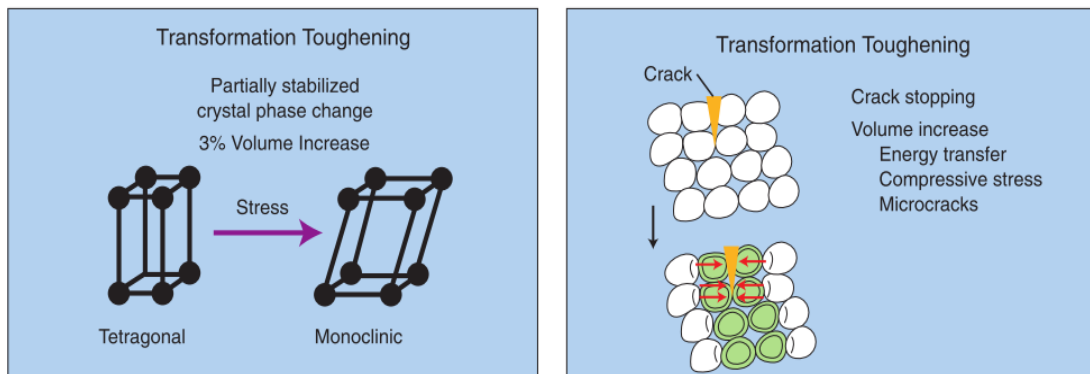


Figure 2.4: Transformation toughening mechanism of zirconia (Edward & Russell, 2005).

The overall  $t \rightarrow m$  transformation takes place in two major stages. First, transition of the lattice structure from tetragonal to monoclinic occurs by shearing displacement of zirconium ions, the second stage involves diffusional migration of oxygen ions to oxygen sites in the monoclinic lattice. The displacement of the oxygen ions from the ideal fluorite positions along the c-axis has been investigated by X-ray diffraction. It was hypothesised that, while the rapid shear displacement of the zirconium ions is the rate controlling factor for nucleation and longitudinal growth of the monoclinic plates, the diffusional migration of the oxygen ions controls the lateral growth of the plates. In the reverse  $m \rightarrow t$  transition, migration of the  $Zr^{4+}$  and  $O^{2-}$  ions to their respective positions is diffusion controlled (Basu, 2005)

These forces can also induce a secondary micro-cracking toughening mechanism in the transformation zone, which generates a network of small, disordered cracks in the zone ahead of a propagating crack. Generation of microcracks ahead of the crack front absorbs and distributes energy among multiple smaller cracks which would otherwise propagate a critical flaw. This microcracking zone can also provide pathways for crack deflection of the advancing crack tip (Barsoum *et al.*, 1992)

## **2.6 Limitation of ZTA**

Despite with the reinforcement of YSZ, the fracture toughness of ZTA only improved to  $\sim 4.5 \text{ MPa}\cdot\sqrt{\text{m}}$  compared to monolithic  $\text{Al}_2\text{O}_3$ :  $3.9 \text{ MPa}\cdot\sqrt{\text{m}}$  (Casellas *et al.*, 2003). Because of this, the performance of ZTA cutting inserts are limited by its fracture toughness. Alternatively, additives were introduced to reduce the sintering temperature, customize the microstructure and improve the product properties.

## 2.7 Magnesium Oxide (MgO)

Magnesium oxide (MgO), or magnesia, is a white hygroscopic solid mineral that occurs naturally as periclase. It has an empirical formula of MgO and consists of a lattice of  $Mg^{2+}$  ions and  $O^{2-}$  ions held together by ionic bonding. Just like ceria, magnesia can be added as stabilizer in zirconia alumina composites to improve their mechanical properties. The incorporation of magnesia into alumina restricts grain growth. This is done by lowering the grain boundary mobility and surface energy of the grains, as well as increasing the surface diffusivity and densification. Hence an increase of density increases the hardness of the ceramics (Wang *et al.*, 1998).

From Azhar *et al.* (2010), addition of MgO into ZTA shown an increase of hardness. In this study, the MgO only affect the grain growth of alumina in the composite but it did not affect yttria stabilized zirconia. As the addition is exceed 0.7 wt.% in a ZTA (with 80 wt.% alumina and 20 wt.% yttria stabilized zirconia), the pinning effect of magnesia decreased as shown in Figure 2.5. Resulting in larger alumina grains and the composite density decreased (Azhar *et al.*, 2010).

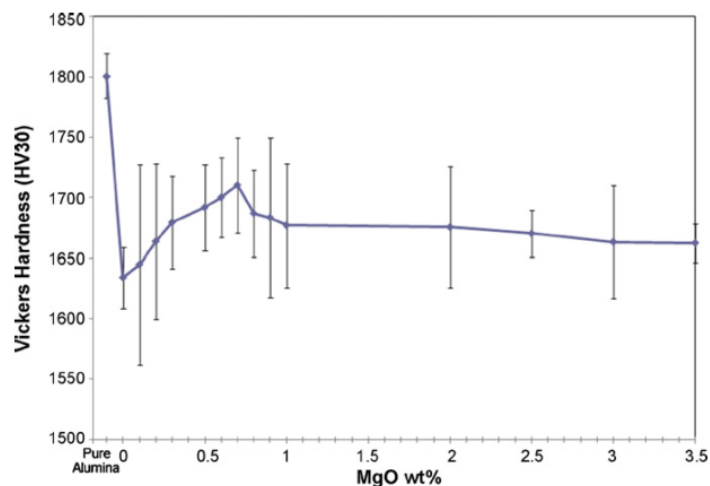


Figure 2.5: Vickers hardness of ZTA ceramics insets as a function of MgO wt.% (Azhar *et al.*, 2010).

As for fracture toughness aspect, there is a decreasing trend with magnesia addition due to the intrinsic nature of low fracture toughness of the oxide. Also, the smaller alumina grain size, the smaller the grain bridge that acts as reduced load bridging capability. The values of hardness and fracture toughness were higher when the addition of MgO was  $> 0.3$  wt.%. Further addition of MgO causes finer grains of  $\text{Al}_2\text{O}_3$  and hence the value of hardness and fracture toughness reduced again. Secondary phase ( $\text{MgAl}_2\text{O}_4$ ) produced due to the addition of MgO more than 0.3 wt.%, which causes the reduction of fracture toughness of ZTA as shown in Figure 2.6.

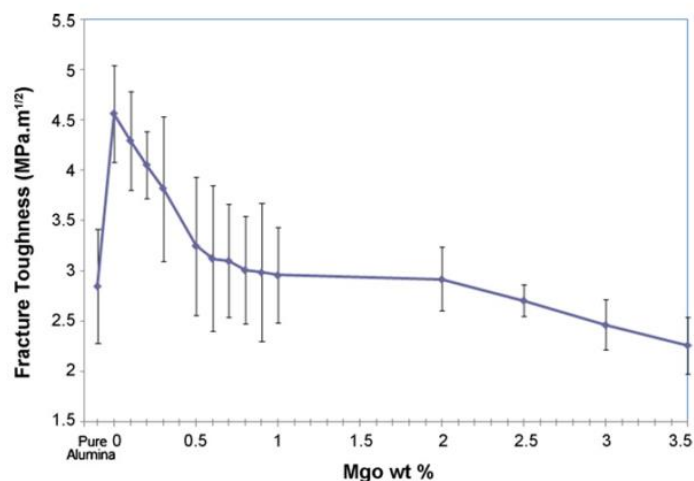


Figure 2.6: Fracture toughness of the ZTA cutting inserts as a function of MgO wt.% (Azhar *et al.*, 2010).

Moreover, Mahmood *et al.* (2017) reported that ZTA/0.5  $\text{TiO}_2$  ceramics with 1.0 wt.% MgO addition under sintering temperature of 1520 °C achieved Vickers hardness of 1637 HV while the fracture toughness is 9.86  $\text{MPa}\cdot\sqrt{\text{m}}$  with improvement of 34% and 29%, respectively. Also, secondary phase of  $\text{MgAl}_2\text{O}_4$  was detected by the XRD analysis when the addition of MgO more than 0.5 wt.%.

## 2.8 Lanthanum Oxide (La<sub>2</sub>O<sub>3</sub>)

Lanthanum oxide is metallic oxide of rare earth element lanthanum, it is La<sup>3+</sup> state in nature and used to develop ferroelectric materials as well as optical materials (Singh, 2010). Other than that, Guo *et al.* (2001), Ai *et al.* (2012), Wu *et al.* (2016), and Naga *et al.* (2016) reported that La<sup>3+</sup> functions as a grain inhibitor during the sintering process as plate like crystals in the samples staggered the grains growth thereby enabling the intergranular bond getting more closer to each other. From Figure 2.7, the Naga *et al.* (2016) found that ZTA ceramics with LaAl<sub>11</sub>O<sub>18</sub> acquired elongated shape. This rod like grain increased with the increased of La<sub>2</sub>O<sub>3</sub> addition into the ZTA ceramics.

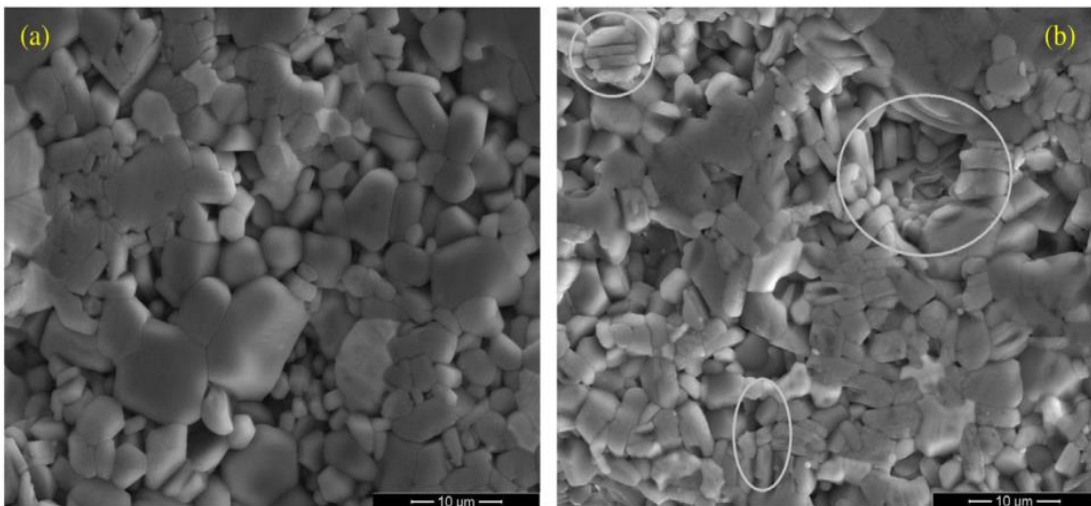


Figure 2.7: SEM images of (a) ZTA ceramics with 12.5 wt.% LaAl<sub>11</sub>O<sub>18</sub>, (b) ZTA ceramics with 37.5 wt.% LaAl<sub>11</sub>O<sub>18</sub> (Naga *et al.*, 2016).

Naga *et al.* (2016) has studied the in-situ sintering reaction of Al<sub>2</sub>O<sub>3</sub>/LaAl<sub>11</sub>O<sub>18</sub>/ZrO<sub>2</sub>. The samples were pressed uniaxially and sintered at 1600 °C up to 1725 °C for 1 hour. From XRD result, the only present phases are alumina, lanthanum hexa-aluminates and zirconia. Also, rod like LaAl<sub>11</sub>O<sub>18</sub> was observed in the sintered bodies containing more than 25 wt.% LaAl<sub>11</sub>O<sub>18</sub>. Increasing the LaAl<sub>11</sub>O<sub>18</sub>

content more than 25 wt.% enhances the fracture toughness but reduces both the bending strength and the hardness of the sintered composites. The results are shown at Figure 2.8.

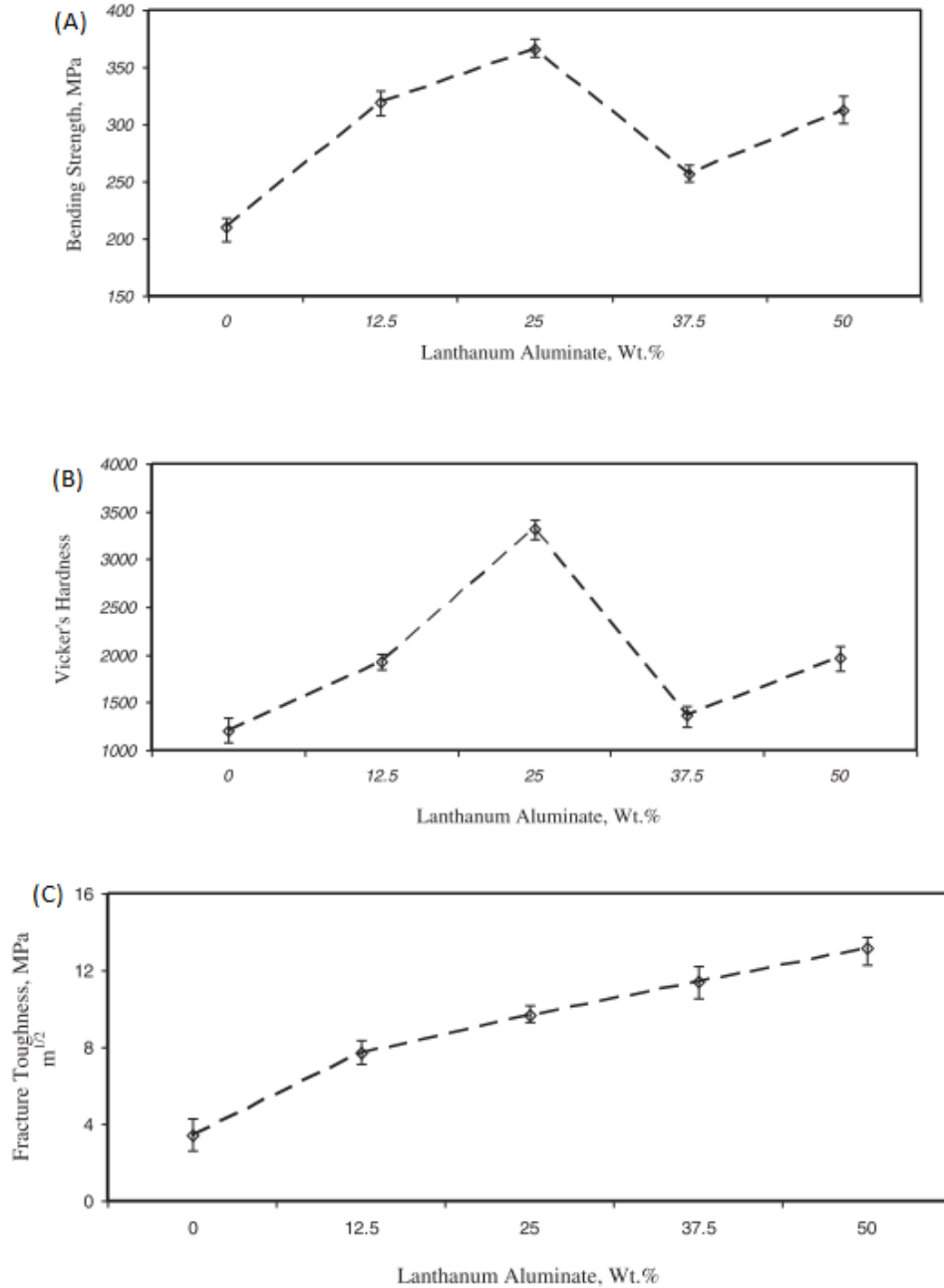


Figure 2.8: Effect of LaAl<sub>11</sub>O<sub>18</sub> content on (a) Bending strength (b) Vickers hardness and (c) Fracture toughness of ZTA composite (Naga *et al.*, 2016).



Besides that, the effects of sintering temperature and the amount of rod-like  $\text{LaAl}_{11}\text{O}_{18}$  were investigated by Guo *et al.* (2001). The mechanical properties of ZTA ceramics were improved by the  $\text{LaAl}_{11}\text{O}_{18}$ , with strength over 500 MPa and fracture toughness  $7 \text{ MPa}\cdot\sqrt{\text{m}}$ . As the  $\text{LaAl}_{11}\text{O}_{18}$  amount increased, part of the t- $\text{ZrO}_2$  transformed to m- $\text{ZrO}_2$ , which is revealed by the decrease in the peak intensity of X-ray diffraction pattern, and which brought about a reduction in hardness and Young's modulus.

## **2.9 Fabrication of ZTA**

From Smuk *et al.* (2003), ZTA ceramic composite with 20 wt.% YSZ are have the optimum mechanical properties. The cutting inserts were fabricated by pressing the mixture at 300 MPa into pellets form then sintered at high temperature 1600 °C in an electrical furnace with constant speed of heating and cooling rate.

Same fabrication methods were used by Azhar *et al.* (2010), Rejab *et al.* (2013), and Hao *et al.* (2010) in their respective research. Monolithic  $\text{Al}_2\text{O}_3$  and YSZ were mixed using a ball mill for 8 hours to ensure homogenous mixture is obtained. The powder was then pressed at 300 MPa with hydraulic press before sintered at 1600 °C for 4 hours with 5 °C/min sintering rate.

Despite cold isostatic pressing (CIP) and hot isostatic pressing (HIP) provide ZTA with more dense and higher bulk density with relatively low porosity, uniaxial pressing was still considered as a favor for those researches as it is simple, fast and economical.

## 2.10 Sintering

Sintering is a thermal treatment that bonds particles together into a solid, coherent structure with mass transport mechanisms taking place mostly at the atomic level. Those mass movements consist of the reduction of total porosity by diffusion followed by material transport, mostly density of a collection of grains increases as material flows into voids, decreasing overall size. The green body has a large surface area relative to its volume, providing the driving force in sintering and hence reduced the free surface energy originating from the surface area of the particles (De Jonghe & Rahaman, 2003).

The microstructure of a powder compact consists of discrete particles initially eventually evolves during sintering. For better understanding, it is better to divide the process into three idealized stages to establish a simple sintering model. The initial stage starts once some degree of atomic mobility is achieved as shown in Figure 2.9 (a). At this stage, sharp concave necks are formed between the individual particles. If coarsening mechanisms are very active, the amount of densification will be small. At the intermediate stage, the microstructure consists of a three-dimensional interpenetrating network of solid particles and continuous, channel-pores as shown in Figure 2.9 (b). This stage is considered valid till ~5-10% porosity and coarsening effect are getting significant. As sintering continues, the channel-like pores break down into isolated, closed voids, indicating the start of the final stage as shown in Figure 2.9 (c). Grain growth can be more extensive at this stage and the removal of the last few percent of porosity is difficult.

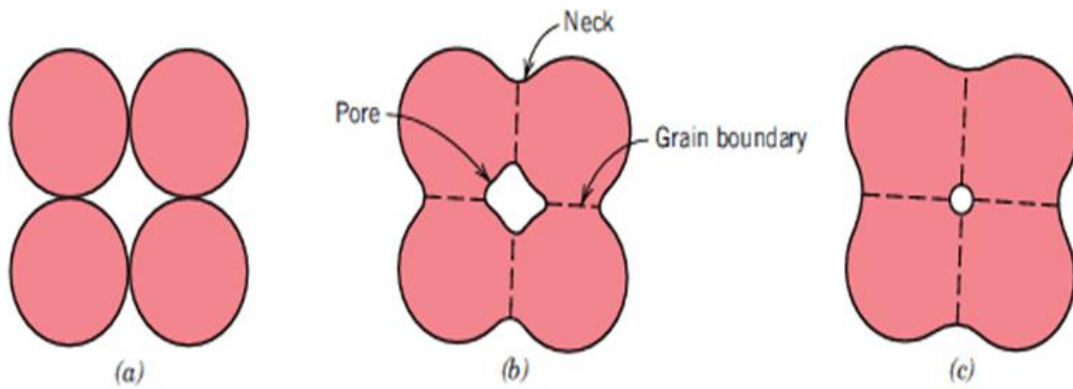


Figure 2.9: For powder compact, microstructural changes during sintering. (a) Powder particles after pressing, (b) Particle coalescence and pore formation as sintering begins and (c) As sintering proceeds, the pores change size and shape (De Jonghe & Rahaman, 2003).

Sintering of crystalline materials can occur by several mechanisms as shown in the Figure 2.10. Densifying and non-densifying mechanisms can be differentiated very clearly. Vapor transport, surface diffusion, and lattice diffusion from the particle surfaces to the neck lead to neck growth and coarsening of the particles without densification. Grain boundary diffusion and lattice diffusion from the grain boundary to the neck are the most crucial densifying mechanisms for polycrystalline ceramics. Diffusion from the grain boundaries to the pores allows neck growth and shrinkage (densification). Plastic flow by dislocation motion can cause neck growth and densification through deformation (creep) of the particles corresponding to the sintering stress. Plastic flow is most common in the sintering of metal powders. For glass powders without grain boundaries, densification and neck growth are done via viscous flow, involving deformation of the particles.

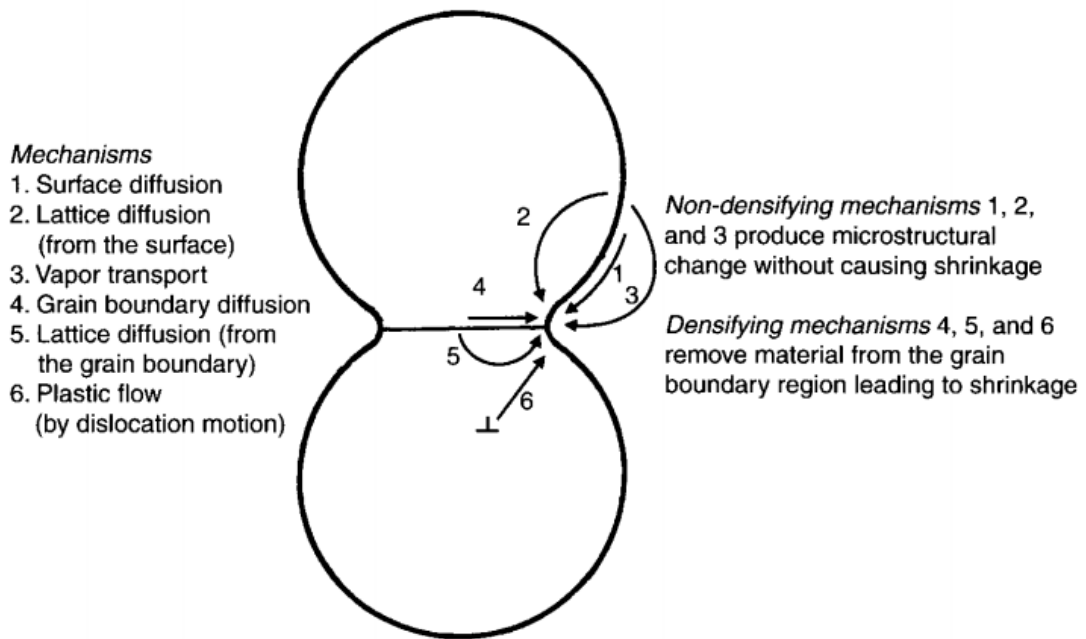


Figure 2.10: Schematic representation of the sintered mechanism for a system of two particles (De Jonghe & Rahaman, 2003)

## 2.11 Uniaxial Pressing Method

Axial pressing is the most important forming method used for ceramic parts. In this process, the powder is compacted between rigid punch faces and die walls, producing compacts with close geometric tolerances. The compaction sequence consists of die filling, compaction, and ejection of the compact as shown in Figure 2.11. The processes are carried out on mechanical or hydraulic compaction presses enabling high production rates. Moreover, axial powder pressing is an economic method for the mass production of precision parts such as cutting tool inserts and sealing disks (Riedel & Chen, 2011)

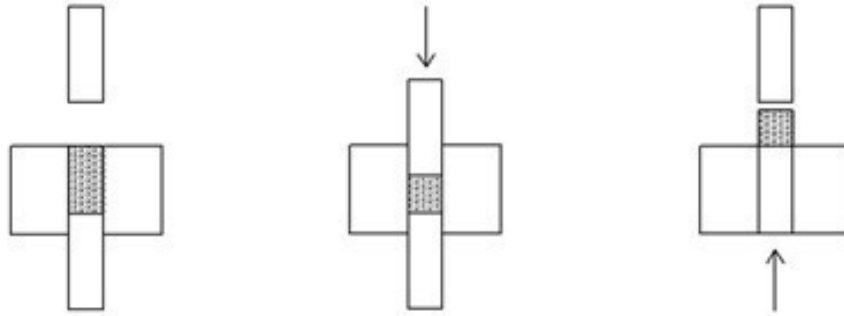


Figure 2.11: Schematic diagram of the uniaxial pressing method (Riedel & Chen, 2012)

## 2.12 Characterization

### 2.12.1 X-ray Diffraction (XRD)

X-ray powder diffraction (XRD) is an analytical technique primarily used for phase identification of a crystalline material and unit cell dimensions. The analyzed material is finely ground, homogenized, and average bulk composition is determined. X-ray diffraction is based on constructive interference of monochromatic X-rays and a crystalline sample. These X-rays are generated by a cathode ray tube, filtered to produce monochromatic radiation, collimated to concentrate, and directed toward the sample. The interaction of the incident rays with the sample produces constructive interference (and a diffracted ray) when conditions satisfy Bragg's Law ( $n\lambda = 2d\sin\theta$ ). This law relates the wavelength of electromagnetic radiation to the diffraction angle and the lattice spacing in a crystalline sample. These diffracted X-rays are then detected, processed and counted. By scanning the sample through a range of  $2\theta$  angles, all possible diffraction directions of the lattice should be attained due to the random orientation of the powdered material. Conversion of the diffraction peaks to d-spacing's allows identification of the mineral because each mineral has a set of unique d-spacing's. Typically, this is achieved by comparison of d-spacing's with standard reference patterns (Callister, 2010).

According to Naga *et al.* (2016), the samples displayed almost similar XRD pattern and they are consisting of  $\text{Al}_2\text{O}_3$ ,  $\text{ZrO}_2$  and  $\text{LaAl}_{11}\text{O}_{18}$  as shown in Figure 2.12. There is no lanthanum zirconate or any other intermediate phases were detected.

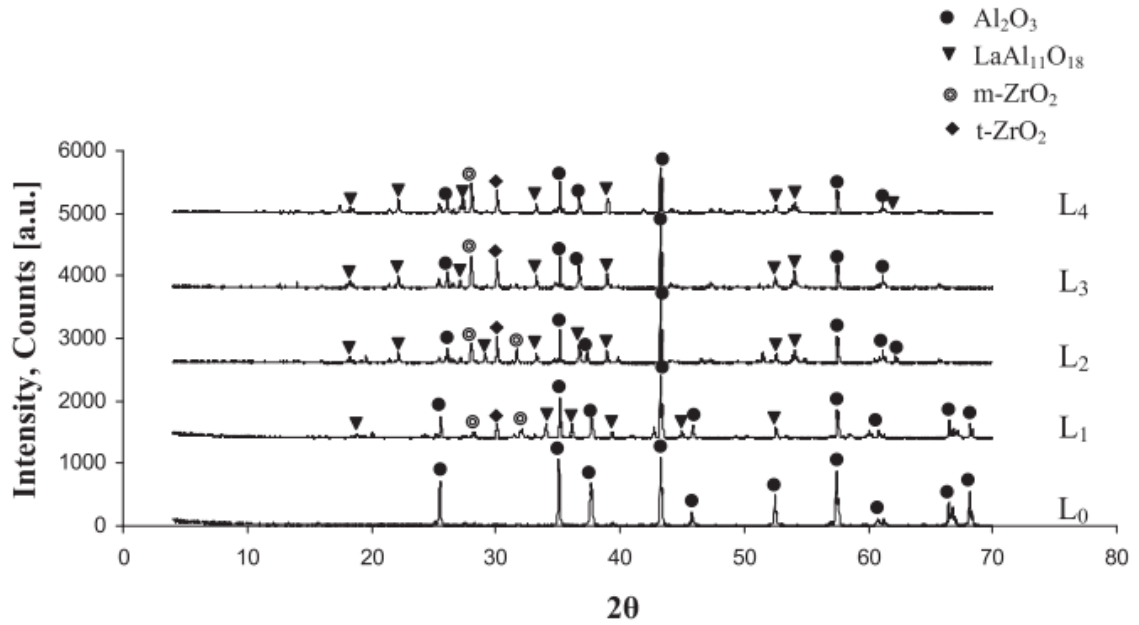


Figure 2.12: XRD pattern of the  $\text{Al}_2\text{O}_3/\text{LaAl}_{11}\text{O}_{18}/\text{ZrO}_2$  ceramics with different content of  $\text{LaAl}_{11}\text{O}_{18}$ : ( $L_0$ ) 0 wt.% of  $\text{LaAl}_{11}\text{O}_{18}$ , ( $L_1$ ) 12.5 wt.% of  $\text{LaAl}_{11}\text{O}_{18}$ , ( $L_2$ ) 25 wt.% of  $\text{LaAl}_{11}\text{O}_{18}$ , ( $L_3$ ) 37.5 wt.% of  $\text{LaAl}_{11}\text{O}_{18}$  and ( $L_4$ ) 50 wt.% of  $\text{LaAl}_{11}\text{O}_{18}$  (Naga *et al.*, 2016)

According to Azhar *et al.* (2010), XRD analysis shown both tetragonal and monoclinic phases as present in YSZ.  $\text{Al}_2\text{O}_3$  XRD result indicates the phase present is corundum. Presence of MgO was recorded as  $\text{MgAl}_2\text{O}_4$  and detectable only when the amount of MgO is more than 1.0 wt.% as shown in Figure 2.13.